Journal of Innate Immunity

Research Article

J Innate Immun 2023;15:765–781
DOI: 10.1159/000533732

Received: September 21, 2022
Accepted: July 20, 2023
Published online: October 5, 2023

Mesenchymal Stromal Cells Facilitate Neutrophil-Trained Immunity by Reprogramming Hematopoietic Stem Cells

Julie Ng[a] Anna E. Marneth[b] Alec Griffith[c] Daniel Younger[c] Sailaja Ghanta[d] Alan Jiao[e] Gareth Willis[d] Junwen Han[a] Jewel Imani[a] Bailin Niu[c] Joshua W. Keegan[c] Brandon Hancock[c] Fei Guo[c] Yang Shi[e] Mark A. Perrella[a, d] James A. Lederer[c]

[a]Division of Pulmonary and Critical Care, Department of Medicine, Brigham and Women's Hospital, Boston, MA, USA; [b]Division of Hematology, Department of Medicine, Brigham and Women's Hospital, Boston, MA, USA; [c]Department of Surgery, Brigham and Women's Hospital, Boston, MA, USA; [d]Department of Pediatric Newborn Medicine, Brigham and Women's Hospital, Boston, MA, USA; [e]Ludwig Institute for Cancer Research, Nuffield Department of Medicine, University of Oxford, Oxford, UK

Keywords
Trained immunity · Epigenetics · Hematopoietic stem cells · Neutrophils · Toll-like receptor 9

Abstract
Novel therapeutics are urgently needed to prevent opportunistic infections in immunocompromised individuals undergoing cancer treatments or other immune-suppressive therapies. Trained immunity is a promising strategy to reduce this burden of disease. We previously demonstrated that mesenchymal stromal cells (MSCs) preconditioned with a class A CpG oligodeoxynucleotide (CpG-ODN), a Toll-like receptor 9 (TLR9) agonist, can augment emergency granulopoiesis in a murine model of neutropenic sepsis. Here, we used a chimeric mouse model to demonstrate that MSCs secrete paracrine factors that act on lineage-negative c-kit+ hematopoietic stem cells (HSCs), leaving them "poised" to enhance emergency granulopoiesis months after transplantation. Chimeric mice developed from HSCs exposed to conditioned media from MSCs and CpG-ODN-preconditioned MSCs showed significantly higher bacterial clearance and increased neutrophil granulopoiesis following lung infection than control mice. By Cleavage Under Targets and Release Using Nuclease (CUT&RUN) chromatin sequencing, we identified that MSC-conditioned media leaves H3K4me3 histone marks in HSCs at genes involved in myelopoiesis and in signaling persistence by the mTOR pathway. Both soluble factors and extracellular vesicles from MSCs mediated these effects on HSCs and proteomic analysis by mass spectrometry revealed soluble calreticulin as a potential mediator. In summary, this study demonstrates that trained immunity can be mediated by paracrine factors from MSCs to induce neutrophil-trained immunity by reprogramming HSCs for long-lasting functional changes in neutrophil-mediated antimicrobial immunity.

karger@karger.com
www.karger.com/jin

Correspondence to:
James A. Lederer, jlederer@bwh.harvard.edu

Introduction

Lower respiratory tract infections are a leading cause of mortality and disability-adjusted life-years worldwide [1] accounting for $13.4 billion in the USA for care related to the index episode [2]. In particular, pulmonary infections exact an unacceptable and disproportionate toll on patients with underlying malignancies, who are at increased risk for severe disease requiring intensive care [3]. Despite advances in cancer care that have improved disease-free and overall survival rates, increasingly aggressive treatments (i.e., high-dose chemoradiation, hematopoietic stem cell transplantation [HSCT]) are often limited by life-threatening pulmonary infections [4, 5]. For example, bacterial pneumonias complicate the course of 15% of patients who undergo HSCT [6]. In the 30 days immediately posttransplant, 10–20% of HSCT patients will require an admission to the intensive care unit, which is associated with high (40–70%) mortality, driven primarily by respiratory failure and infection [7, 8]. These patients are at high risk for opportunistic infections, for which there are currently no preventative strategies beyond antibiotics [6]. In an era of growing antimicrobial resistance [9], this is an unsustainable approach. New strategies aimed at prophylaxis to reduce the burden of disease from severe respiratory infections are urgently needed.

Mesenchymal stromal cells (MSC) are fibroblast-like cells defined by in vitro plastic adherence, trilineage (osteoblast, adipocyte, and chondroblast) differentiation potential, negative immune lineage markers, and positive mesenchymal markers [10]. They play a pivotal role in the hematopoietic niche [11] and can modulate the bone marrow [12] and neutrophil response to infection [13]. We have previously demonstrated that prophylactically administering MSCs preconditioned with CpG oligonucleotides (CpG; hypomethylated GC dinucleotides highly enriched in bacterial genomes) to sublethally irradiated mice conferred a survival benefit when the mice were subsequently intranasally infected with *Pseudomonas aeruginosa* [14]. This was associated with enhanced emergency granulopoiesis, or the de novo generation of neutrophils in response to a systemic infection [15], and increased myeloid differentiation and proliferation potential in c-kit+ hematopoietic stem cells (HSCs). Notably, there was a near equivalent effect on myelopoiesis when mice were given MSC-conditioned media (CdM) alone, compared to whole cells, suggesting that paracrine factors secreted by MSCs and CpG-MSCs in the CdM can augment emergency granulopoiesis. However, the mechanisms underlying this protective effect, and the longevity of this effect, remain unelucidated.

Epidemiological data show that live attenuated vaccines such as Bacille Calmette-Guérin (BCG) [16], a weakened form of *Mycobacterium tuberculosis*, have heterologous effects that reduce all-cause infectious mortality, particularly from sepsis and severe respiratory infections [17, 18]. Research into this phenomenon has led to the discovery of trained immunity, a type of innate immune memory whereby microbial ligands can functionally reprogram innate immune cells leading to an enhanced response when challenged with a subsequent infection [19]. Due to the short half-lives of mature innate cells such as monocytes and neutrophils [20, 21], reprogramming in these populations occurs via epigenetic and/or metabolomic changes in hematopoietic stem and progenitor cells that are passed on when they differentiate into mature effector cells [22]. Despite the well-established importance of bone marrow niche cells such as MSCs in maintaining and dictating HSC fate and function [23, 24], the potential role for MSC paracrine factors in trained immunity has not yet been explored. This study adds on our previously published data and explores the potential role of paracrine factors from MSCs as mediators of neutrophil-trained immunity.

Methods

MSCs and CdM

Human bone-derived MSCs were purchased from the Center for the Preparation and Distribution of Adult Stem Cells at the Texas A&M University Health Science Center as previously described [14]. These cells were from a de-identified individual and were prepared under an IRB-approved protocol from consented donors. Since these cells were purchased as de-identified cell lines, endotoxin testing was performed on whole cell lysates and reagents using the *Limulus* amebocyte lysate chromogenic endotoxin assay kit (Pierce), demonstrating <0.5 EU/mL. Passage 5–8 MSCs were cultured in alpha-MEM media (Gibco) supplemented with 20% fetal bovine serum (Gibco, FBS) and 1% Antibiotic-Antimycotic (Thermo Fisher Scientific) until 80–90% confluency. CpG-MSCs were conditioned with 3 μg/mL CpG-ODN 2336 (InvivoGen) for 30 min. Cells were washed 3 times with phosphate buffer saline (PBS) prior to incubation in supplement-free alpha-MEM media for 24 h. CdM was collected and concentrated using Amicon Ultra-15 centrifugal filter units with 3 KDa cutoff (Millipore) as per manufacturer's instructions.

Chimeric Mouse Model

Male 6–8-week-old CD45.1 expressing CByJ.SJL(B6)-*Ptprc*^{a}/J mice (Strain #006584) were purchased from Jackson Laboratory (Bar Harbor, ME, USA). CD45.1 lineage-negative c-kit+ cells were isolated from compact bones by negative selection using

biotinylated anti-mouse CD3 (Biolegend clone 145-2C11), B220 (Biolegend clone RA3-6B2), GR-1 (Biolegend clone RB6-8C5), CD11b (Biolegend clone M1/70), NKp46 (Biolegend clone 29A1.4), and TER-119 (Biolegend TER-119) with anti-biotin microbeads (Miltenyi Biotec) through an LD magnetic column (Miltenyi Biotec), followed by positive selection with PE anti-mouse c-kit (Biolegend clone 2B8) with anti-PE microbeads (Miltenyi Biotec) through an MS magnetic column (Miltenyi Biotec). The purity of c-kit+ cells was confirmed to be >90% by flow cytometry using a MACSQuant Analyzer 10 flow cytometer and analyzed using FlowJo software (Tree Star Inc.). C-kit+ cells were cultured for 48 h ex vivo in StemSpan SFEM II (STEMCELL Technologies) supplemented with 50 ng/mL thrombopoietin (PeproTech), 100 ng/mL stem cell factor (PeproTech), and 30% of either (1) MSC-CdM (3×10^5 cell equivalent), (2) CpG-MSC-CdM (3×10^5 cell equivalent), or (3) alpha-MEM media control at 37°C with 5% CO_2. Recipient CD45.2 expressing 8-week-old male BALB/cByJ mice (Strain #000651) were purchased from Jackson Laboratories (Bar Harbor, ME, USA) and lethally irradiated with 9 Gy radiation in 2 doses spaced 12 h apart using a Gammacell 40 Exactor Cesium-137 dual-source irradiator (Best Theratronics). 1.5–2 × 10^5 c-kit+ cells in 150 μL PBS [25] from one of the described three conditions were transplanted by retro-orbital injection. Six weeks after transplantation, peripheral blood chimerism was determined by flow cytometry using FITC-CD45.1 (Biolegend, clone A20) or FITC-CD45.2 (Biolegend, clone 104), APC-Cy7-B220 (Biolegend, clone RA3-6B2), PE-CD3 (Biolegend clone 145-2C11), APC-Ly6G (Biolegend clone 1A8), and Pacific Blue-CD11b (Biolegend clone M1/70).

Mouse Model for Sublethal Radiation and Infection

A 2-hit experimental model for total body irradiation with lung bacteria challenge infection was used as previously described [14]. 8–10-week-old male CD-1 mice (Charles River) were irradiated with 5 Gy radiation. On day 3, retro-orbital injections of (1) PBS vehicle control, (2) CpG-MSC-CdM (equivalent to 2.5 × 10^5 cells), (3) extracellular vesicles (EVs) from CpG-MSCs (equivalent to 2.5 × 10^5 cells), or (4) EV-free soluble fraction (EVFSF) from CpG-MSCs (equivalent to 2.5 × 10^5 cells). On day 7, animals were intranasally infected with 1–2 × 10^6 colony-forming units (CFU) of *P. aeruginosa* (ATCC strain 27853). Then, 6 h later, a second dose of one of the above conditions was given by tail vein injection. Mice were sacrificed 48 h after infection for functional analyses.

Quantification of Organ Bacterial Burden

Sixteen weeks after transplantation, chimeric mice were intranasally infected with 1–1.5 × 10^7 CFU of *Pseudomonas* (*P.*) *aeruginosa* in 40 μL PBS. Then, 24 h after infection, mice were sacrificed and the whole left lung or whole spleen were harvested into 1 mL of PBS and homogenized using a tissue homogenizer (Tissue-Tearor, BioSpec Products). Serial dilutions of each sample were plated onto Luria Broth agar overnight and at 37°C, and bacterial CFU were quantified the following day.

Plasma Cytokine Analysis

Whole blood was obtained by cardiac puncture after death and collected in EDTA-containing microtainer tubes (BD Biosciences). Samples were centrifuged for 15 min at 2,000 × *g* and the supernatant was collected and stored at −80°C until use. 40 μL of undiluted sample was used for analysis by Luminex FlexMap 3D assay system as per manufacturer's instructions.

Cobblestone Area-Forming Cell Assay

The cobblestone area-forming cell (CAFC) assay was setup as previously described [26]. MS-5 (DSMZ, # ACC 441) murine stromal cells were cultured in alpha-MEM with 10% FBS, 2 mM L-glutamine, and 1% antibiotic-antimycotic in 12-well plates (Sigma-Aldrich) until confluent. Lineage-negative, sca-1+, c-kit+ (LSK) cells were isolated from male mice by fluorescence-activated cell sorting using a FACSAria III cell sorter (BD Biosciences). 1,000 LSK cells were seeded per well in Myelocult 5300 (STEMCELL Technologies) and incubated at 37°C with 5% CO_2 for 7–9 days until "cobblestone" areas were visualized by phase-contrast illumination. After visualizing cobblestone areas, 50 μL of (1) MSC-CdM (equivalent to 5 × 10^5 cells), (2) CpG-MSC-CdM (equivalent to 5 × 10^5 cells), or (3) alpha-MEM media control was added to the culture for 24 h. The cultures were gently washed twice with PBS, and fresh Myelocult 5300 was added to each well. Live neutrophils were harvested weekly from the supernatant and phagocytosis assays were performed. Technical replicates were performed in triplicate.

Colony-Forming Assays

Single-cell suspensions of bone marrow hematopoietic cells were prepared by lysing with ammonium chloride solution and centrifugation at 100 × *g* for 10 min to remove platelets. Lineage-negative c-kit+ cells were isolated as described above and counted by flow cytometry. 1,000 c-kit+ cells were seeded into 1 mL of MethoCult GF M3434 (STEMCELL Technologies) and incubated at 37°C with 5% CO_2 for 9 days prior to blinded scoring of phenotypically identified colonies based on colony appearance and flow cytometry validation by staining with anti-F4-80 antibody to identify macrophages and anti-Ly6-G antibody to identify neutrophils as previously described [14]. Technical replicates were performed in triplicate, and the results of separate experiments were pooled after standardization by fold change relative to the total number of colonies per plate in control groups.

Phagocytosis Assay

Green fluorescent protein-labeled *P. aeruginosa* (gifted by Dr. Gerald Pier) opsonized with 10% serum for 30 min was added to neutrophils at a multiplicity of infection of 100 bacteria per neutrophil and incubated at 37°C for 2 h. At the end of the assay, cells were immediately fixed with 4% paraformaldehyde for 15 min, scraped off the plate, quenched with trypan blue, and stained with APC-Ly6G (Biolegend clone 1A8) prior to analysis by flow cytometry.

Isolation of EV and EVFSF

EVs were isolated by ultra-centrifugation as previously described [27]. CdM was prepared as described above in 8 mL of supplement-free alpha-MEM. HEPES (Gibco) was added to CdM to obtain a final concentration of 25 mM. CdM was centrifuged at 300 × *g* for 10 min, followed by 2,000 × *g* for 10 min at 4°C prior to filtration through a 0.22 μm syringe filter (EMD Millipore) to remove apoptotic bodies and debris. The CdM was then ultra-centrifugated at 10,000 × *g* for 75 min at 4°C. The resultant

supernatant was saved as the EVFSF. The pellet was resuspended in cold PBS and centrifuged at 10,000 × *g* for 75 min at 4°C. The supernatant was discarded, and the pellet was resuspended in PBS for further use.

Characterization of EVs

EVs were characterized as outlined by the International Society for Extracellular Vesicles [28] prior to use. For Western blot analysis, EVs and whole cells (positive control) were lysed in ×1 RIPA buffer (Cell Signaling) and ×1 mini protease inhibitor cocktail (Roche). Laemmli's SDS sample buffer (Boston BioProducts) was added, and the samples were boiled at 100°C for 5 min prior to loading equal protein concentrations onto a 4–20% Mini Protein TGC Gel (Bio-Rad laboratories). Antibodies for blotting included CD90 (Biolegend clone 5E10), CD73 (Biolegend clone AD2), CD105 (Biolegend 43A4), and calnexin (Santa Cruz Biotechnology). Transmission electron microscopy was performed on EVs by absorbing an aliquot of EVs onto a formvar/carbon grid, staining with 2% uranyl acetate, and visualizing on a JEOL 1200EX TEM as previously described [29]. Nanoparticle tracking analysis was performed on EVs using NanoSight LM10 System (Malvern Instruments).

Signaling Mass Cytometry

Cell cultures from the CAFC assay were grown until visualization of cobblestone areas. Cultures were then stimulated with 50 μL of 1) alpha-MEM media control, 2) MSC-CdM (equivalent to 5×10^5 cells), 3) CpG-MSC-CdM (equivalent to 5×10^5 cells), or 4) 10 μg/mL lipopolysaccharide for 1, 5, and 30 min. Cells were immediately fixed in Smart Tube proteomic stabilizer for 10 min (Smart Tube Inc.). Smart Tube ×1 thaw-lyse buffer was added to the cells for 10 min, twice, before the cells were spun down at 600 × *g* for 5 min as per manufacturer's protocol. Cells were incubated in Foxp3/Transcription Factor Fixation/Permeabilization buffer (Invitrogen) for 30 min and transferred to a polypropylene 96-well plate. The samples were incubated with SCN-EDTA-coupled palladium-based barcoding reagents for 15 min and then combined into a single sample tube. Conjugated antibodies (used at a 1:100 dilution in Permeabilization buffer, unless stated otherwise) were added into each tube and incubated for 60 min. Cells were then fixed with 4% formaldehyde for 10 min. Immediately before samples were acquired, DNA was labeled for 20 min with a 4.75 μM iridium intercalator solution (Fluidigm), to identify single cell events. Samples were subsequently washed and reconstituted in Cell Acquisition Solution (Fluidigm) in the presence of EQ Four Element Calibration beads (Fluidigm) at a final concentration of 1×10^6 cells/mL. Samples were acquired on a Helios CyTOF Mass Cytometer (Fluidigm). Mass cytometry data were debarcoded [30], normalized [31], and analyzed using OMIQ online software (https://www.omiq.ai/) to perform optimized t-Distribution Stochastic Neighbor Embedding (optSNE) analysis on files equal sampled to 100,000 events. Clustering was performed using weighted Phenotyping by Accelerated Refined Community partition (PARC) [32], and bifurcating developmental trajectories were identified with Wishbone [33] using a random LSK cell as a starting point. Heatmaps of expression levels of each channel for each cluster were generated in GraphPad Prism software.

CUT&RUN

Live c-kit+ cells from chimeric mice were stained using Zombie Violet fixable viability kit (Biolegend) and APC-c-kit (Biolegend clone 2B8). Sorting for live c-kit+ cells was performed using a FACSAria III cell sorter (BD Biosciences). Cleavage Under Targets and Release Using Nuclease (CUT&RUN) was performed on equal numbers of c-kit+ cells from each group of chimeric mice using the CUT&RUN Assay Kit (Cell Signaling, Kit #86652) as per manufacturer's protocol. Chromatin associated with H3K4me3 (Cell Signaling, clone C42D8), and rabbit IgG-negative isotype control (Cell Signaling, clone DA1E) were isolated. Technical replicates were performed in duplicate. CUT&RUN sequencing was performed by the Molecular Biology Core Facilities at Dana-Farber Cancer Institute. CUT&RUN libraries were prepared using Swift S2 Acel reagents on a Beckman Coulter Biomek i7 liquid handling platform from approximately 1 ng of DNA according to manufacturer's protocol and 14 cycles of PCR amplification. Finished sequencing libraries were quantified by Qubit fluorometer and Agilent TapeStation 2200. Library pooling and indexing were evaluated with shallow sequencing on an Illumina MiSeq. Subsequently, libraries were sequenced on a NovaSeq with 150-bp paired-end reads. Adapters were trimmed using TrimGalore! (v0.6.6) and Cutadapt (v1.8.1). Sequences were aligned using Bowtie2 (v2.4.1) [34] to the mm10 mouse reference genome. SAM files were converted to BAM files using Samtools (v1.4.1). Sorted BAM files were converted to bigwig files using bamCoverage, part of the deepTools suite (v3.1.2) [35] and visualized with the Integrative Genomics Viewer from the Broad Institute and University of California, San Diego. Quality was assessed using the ChIPQC R package [36], as described by the ENCODE consortium. Peaks were called using MACS2 (v2.1) [37] and the concordance of peak calls between replicates was assessed using the Irreproducibility Discovery Rate framework [38] (v2.0.3). Replicates were combined using BEDtools (v2.26.0) [39], and genes were annotated using the ChIPseeker R package [40] using the full genome sequences for *Mus musculus* (UCSC version mm10). Functional enrichment of the obtained gene annotations for peak calls for Gene Ontology biological processes and KEGG pathways was performed using the clusterProfiler R package [41, 42].

Proteomic Analysis

CdM was prepared as described above. CdM was harvested and protease inhibitor cocktail (Roche) was added as per manufacturer's instructions. CdM was centrifuged at 5,000 × *g* for 30 min at 4°C and the supernatant was concentrated using Amicon Ultra-15 centrifugal filter units with 3 KDa cutoff (Millipore). CdM was stored at −80°C until proteomic analysis, which was performed by the Thermo Fisher Center for Multiplexed Proteomics at Harvard Medical School [43]. Briefly, 20% sodium dodecyl sulfate was added to samples to a final concentration of 1%, reduced with tris (2-carboxyethyl) phosphine and alkylated with iodoacetamide. 100 μL of each sample was precipitated by methanol/chloroform and protein pellets were resuspended in 200 mM EPPS (pH 8.0). Digestion was performed sequentially using LysC (1:50) and Trypsin (1:100) based on protease-to-protein ratio. Peptides were labeled with TMT10 reagents, cleaned by SepPak, and dried by SpeedVac. Dried samples were resuspended and fractionated by basic reverse-phase high-performance liquid chromatography. Twelve fractions from the total proteome high-pH reverse-phase set were analyzed on an Orbitrap Eclipse mass spectrometer using

a 90-min method MS3 method. Peptides were detected (MS1) and quantified (MS3) in the Orbitrap. Peptides were sequenced (MS2) in the ion trap. MS2 spectra were searched using the SEQUEST [44] algorithm against a composite database containing the Uniprot human reference proteome. Peptide spectral matches were filtered to 1% false discovery rate using the target-decoy strategy combined with linear discriminant analysis. Proteins were quantified only from peptides with a summed signal/noise threshold of ≥100. Technical replicates were performed in quintuplicate. The top 10 proteins were inputted into Search Tool for the Retrieval of Interacting Genes/Proteins (STRING), a database of known and predicted protein-protein interactions [45].

Results

Chimeric Mice Repopulated with CpG-Bone Marrow Have Increased Myelopoiesis and Improved Bacterial Clearance after Pseudomonas aeruginosa *Pulmonary Infection*

To study the in vivo effects of MSC- and CpG-MSC-CdM on c-kit+ stem cells longitudinally, we generated chimeric mice as described [46] (Fig. 1a). Lineage-negative c-kit+ cells were cultured ex vivo for 48 h in StemSpan SFEM II supplemented with 50 ng/mL thrombopoietin, 100 ng/mL stem cell factor, and 30% of either (1) alpha-MEM media control, (2) MSC-CdM from 3×10^5 cells, or (3) CpG-MSC-CdM from 3×10^5 cells and then transplanted into lethally irradiated recipients. Six weeks after transplantation, peripheral blood donor chimerism and immune cell populations were assessed by flow cytometry. At this time, the mice demonstrated 90% donor chimerism (online suppl. Fig. 1A; for all online suppl. material, see https://doi.org/10.1159/000533732), whereas most of the remaining recipient immune cells were T cells (online suppl. Fig. 1B), likely representing lymphocytes residing within the lymph nodes that survived total body irradiation. Interestingly, there was an increased proportion of peripheral blood neutrophils in the mice transplanted with c-kit+ cells cultured with CpG-MSC-CdM (CpG-BM), compared to MSC-CdM (MSC-BM), and media control (Ctrl-BM) (Fig. 1b). Notably, by 12 weeks after transplantation (Fig. 1c), after which all functional experiments were performed, there was no significant difference in the proportions of peripheral blood populations between the three groups. Plasma cytokines between the mice in the three groups at 12 weeks were also similar (Fig. 1d), suggesting a return to a comparable basal homeostatic level following transplantation [47]. However, c-kit+ cells isolated from the chimeras 12–16 weeks after transplantation demonstrated an increase in myeloid differentiation and proliferation potential as measured by increased numbers of granulocyte/macrophage colony-forming units (CFU-GMs; Fig. 1e) in the mice transplanted with CpG-BM compared to MSC-BM and Ctrl-BM. In contrast, CFU-G and CFU-M were not significantly different between chimeras transplanted with CpG-BM, MSC-BM, or Ctrl-BM. This suggests that despite similar peripheral blood phenotypes, an increased capacity for myelopoiesis persists in mice transplanted with CpG-BM.

To evaluate whether this increased myelopoiesis potential translated to improved bacterial clearance, we infected the chimeras intranasally with 1×10^7 CFUs of *P. aeruginosa* 12–16 weeks after bone marrow transplantation and harvested the whole left lung and whole spleen to assess bacterial clearance at the site of infection (lung) and spread to distal organs (spleen). Mice transplanted with CpG-BM had fewer bacterial CFUs in the lungs (Fig. 1f), and a trend toward decreased bacterial burden in the spleen (Fig. 1g) compared to mice transplanted with Ctrl-BM. This was also associated with an increase in the number of peripheral CD45.1 (donor) neutrophils in the mice transplanted with CpG-BM in response to infection, compared to mice transplanted with Ctrl-BM (Fig. 1h), suggesting that enhanced emergency granulopoiesis was playing a role in improved organ bacterial clearance. Notably, at the time of infection, >95% of the peripheral blood population in the chimeras were donor-derived (online suppl. Fig. 1C). Despite an increased number of neutrophils, infected chimeras transplanted with CpG-BM had lower levels of IL-6 and IL-17A compared to both infected chimeras transplanted with MSC-BM and Ctrl-BM (Fig. 1i), suggesting that the augmented granulopoiesis was not arising from a persistent, dysregulated cytokine response that can be seen in severe sepsis [48, 49], but rather, as an appropriate and enhanced response that can more effectively clear bacteria.

While there was a trend toward, but not a statistical difference in, decreased organ bacterial clearance and increased peripheral neutrophils between chimeras with MSC-BM and CpG-BM, we hypothesized that the difference in plasma cytokines after infection could additionally be driven by enhanced antimicrobial function. To answer this question, we developed an in vitro model based on the cobblestone area-forming cell assay [26, 50] to allow for the longitudinal study of neutrophils derived from LSK cells stimulated once with media control or CdM (Fig. 1j). LSK cells were co-cultured with MS-5 stromal cells until visualization of phase-dark cobblestones under

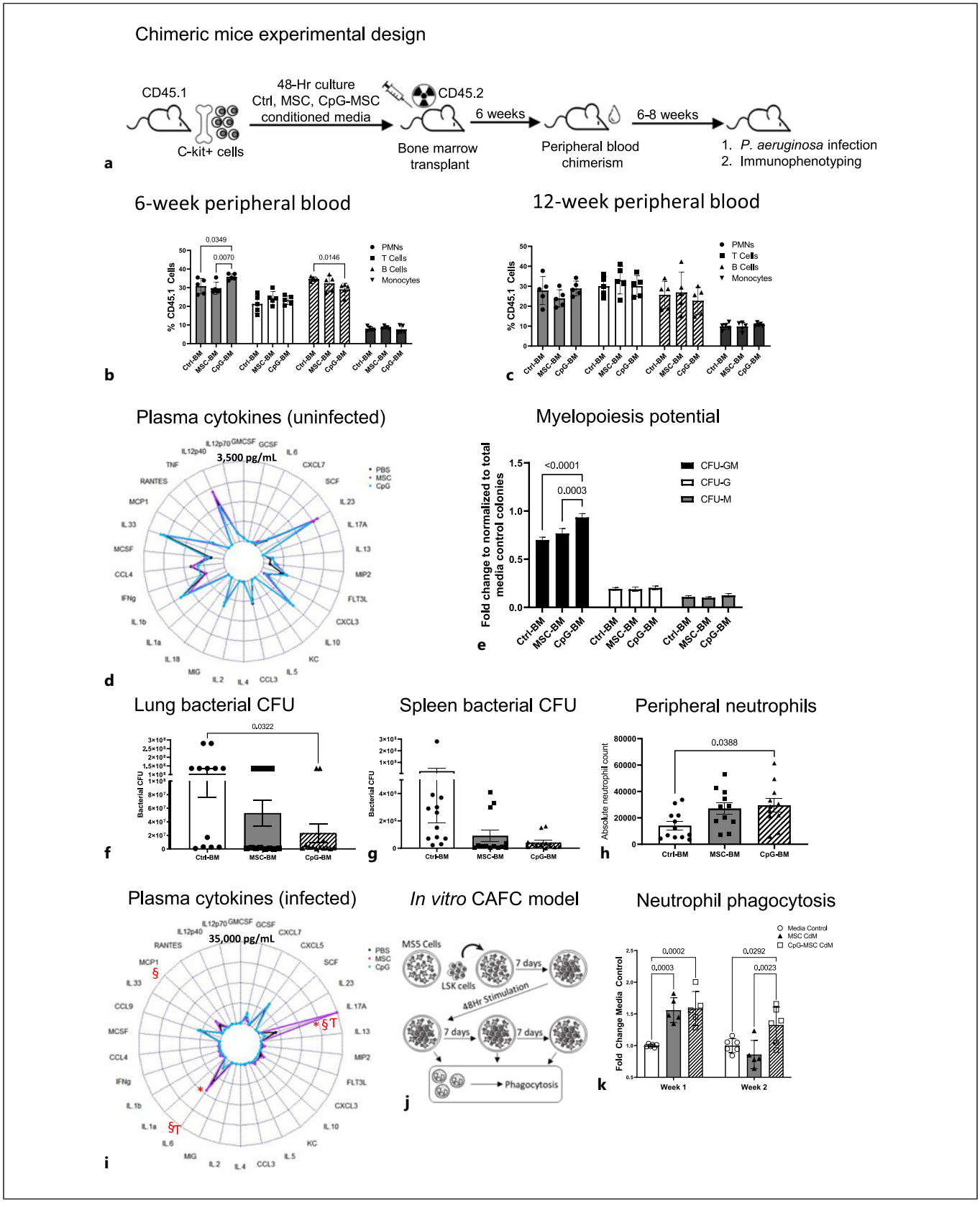

1

(For legend see next page.)

phase-contrast microscopy (online suppl. Fig. 1D), indicative of asymmetric division of the LSK stem cells to both replenish the pool of stem cells in vitro, as well as generation of myeloid cells into the supernatant. The co-cultures are then stimulated with either (1) media control, (2) MSC-CdM, or (3) CpG-MSC-CdM for 48 h. Cultures are then carefully washed with PBS before the addition of fresh media. Neutrophils were collected from the supernatant on a weekly basis and subjected to phagocytosis assays with *P. aeruginosa* expressing green fluorescent protein opsonized with heat-inactivated autologous serum (online suppl. Fig. 1E; Fig. 1k). Neutrophils derived from LSK cells stimulated with both MSC (▲, gray bar) and CpG-MSC (□, striped bar) CdM have increased phagocytosis compared to media control (○, white bar) 1 week after a 48-h stimulation. However, it is only in the neutrophils derived from c-kit+ cells stimulated with CpG-MSC-CdM that this increased phagocytosis was maintained, 2 weeks after stimulation.

CdM Induces Long-Term Epigenetic Modifications in Histone Methylation in c-kit+ Cells

Phenotypic traits can be passed on to progeny by altering gene accessibility to perpetuate specific gene programs and functional states [51]. Many inflammatory genes are tightly regulated by histone modifications [52], and genome-wide trimethylation of the 4th lysine of histone 3 (H3K4me3) has been associated with neutrophil-trained immunity induced by BCG [53]. These epigenetic marks, notably the persistence of H3K4me3 at enhancer and promoter regions [54], leave cells "poised" to allow a stronger response to a secondary infection [55–57]. Therefore, we performed a whole-genome assessment of the distribution of H3K4me3 by CUT&RUN followed by sequencing in c-kit+ cells from the chimeras 16 weeks after transplantation. CUT&RUN was used instead of ChIP-seq, as it allowed for the use of fewer cells [58]. Quality metrics per ENCODE guidelines for ChIP-seq [59] (as there are currently no guidelines for CUT&RUN) were performed (online suppl. Table 1; online suppl. Fig. 2).

Fig. 1. Chimeric mice repopulated with CpG-bone marrow have increased myelopoiesis and improved bacterial clearance after *Pseudomonas aeruginosa* pulmonary infection. **a** Schematic of experimental model. C-kit+ cells were harvested from CD45.1-expressing CByJ.SJL(B6)-*Ptprc*^{a}/J mice and cultured ex vivo for 48 h in StemSpan SFEM II and 30% of (1) alpha-MEM media control, (2) MSC-conditioned media (CdM), or (3) CpG-MSC-CdM. CD45.2-expressing wild-type BALB/cJ mice were lethally irradiated with 9 Gy in 2 divided doses, and 1.5–2 × 10^5 c-kit+ cells from the above conditions in 150 μL PBS were injected retro-orbitally. Peripheral blood chimerism was determined 6 weeks after transplantation. Functional studies, including intranasal *P. aeruginosa* infection, was performed 12–14 weeks after transplantation. Peripheral blood chimerism 6 weeks (**b**) (n = 5 mice per group) and 12 weeks (**c**) (n = 5 mice per group) after bone marrow transplantation. There was an increase in the proportion of neutrophils in the peripheral blood of mice that received c-kit+ cells cultured with CpG-MSC-CdM (CpG-BM), compared to MSC-CdM (MSC-BM), and media control (Ctrl-BM) 6 weeks after transplantation. Data were analyzed by 2-way analysis of variance (ANOVA), interaction $p = 0.003$, and significant comparisons by Bonferroni's multiple comparisons test are denoted on the graph (Ctrl-BM vs. CpG-BM neutrophils, $p = 0.0349$; MSC-BM vs. CpG-BM neutrophils, $p = 0.0070$; Ctrl-BM vs. CpG-BM B cells, $p = 0.0146$). At 12 weeks after transplantation, there was no significant difference in the peripheral blood cell populations. **d** Radar plot showing the mean value of plasma Luminex cytokines in uninfected chimeras (n = 5 in Ctrl-BM [●] and MSC-BM [●], n = 4 in CpG-BM [●]). **e** 1,000 c-kit+ cells isolated from the bone marrow chimeric mice (n = 6 per group) 12–16 weeks after transplantation were seeded into methylcellulose media. Cultures were grown for 9 days prior to blinded manual determination of CFU containing granulocyte macrophages (CFU-GM, black bars), granulocytes (CFU-G, white bars), or macrophages (CFU-M, gray bars). Data were assessed by two-way ANOVA, interaction p = 0.0009. Significant comparisons of CFU-GMs by Bonferroni's multiple comparisons test are denoted on the graph (Ctrl-BM vs. CpG-BM, $p < 0.0001$; MSC-BM vs. CpG-BM, $p = 0.0003$). Sixteen weeks after bone marrow transplantation, chimeras were intranasally infected with 1–1.5 × 10^7 CFU of *Pseudomonas* (*P.*) *aeruginosa* and sacrificed 24 h after infection. The whole left lung (**f**) and whole spleen (**g**) were removed from mice transplanted with CpG-BM (n = 13, ▲), MSC-BM (n = 12, ■), or Ctrl-BM (n = 12, ●), homogenized in 1 mL PBS and plated on onto LB agar overnight prior to quantification of organ bacterial colonies. Data were assessed by one-way ANOVA (lung bacterial organ CFU interaction $p = 0.0347$, spleen bacterial organ CFU interaction $p = 0.3278$). Significant comparisons of lung bacterial organ CFU by Bonferroni's multiple comparisons test are denoted on the graph (Ctrl-BM vs. CpG-BM, $p = 0.0322$). **h** Peripheral blood neutrophils were assessed in infected chimeras by flow cytometry. Data were assessed by one-way ANOVA, interaction $p = 0.0274$. Significant comparisons by Bonferroni's multiple comparisons test are denoted on the graph (Ctrl-BM vs. CpG-BM, $p = 0.0388$). **i** Radar plot showing the mean value of plasma Luminex cytokines in infected chimeras (n = 5 Ctrl-BM [●] and CpG-BM [●], n = 3, MSC-BM [●]). Data were analyzed by 2-way ANOVA, interaction $p < 0.0001$. Significant comparisons by Bonferroni's multiple comparisons test are denoted on the graph (Ctrl-BM vs. CpG-BM [* $p = 0.0027$ for IL-17A, $p < 0.0001$ for IL-6], Ctrl-BM vs. MSC-BM [† $p < 0.001$ for IL-17A, $p = 0.0449$ for IL-6], MSC-BM vs. CpG-BM [§ $p = 0.008$ for MCP-1, $p < 0.0001$ for IL-17A, $p < 0.001$ for IL-6]). **j** Schematic of the in vitro cobblestone area-forming assay (CAFC) for assessing the influence of MSC- and CpG-MSC-CdM on neutrophil function. **k** Neutrophils derived from LSK cells stimulated by media control (○, white bar), MSC-conditioned media (CdM) (▲, gray bar), and CpG-MSC-CdM (□, striped bar) were co-cultured with *P. aeruginosa* expressing green fluorescent protein for 2 h, and phagocytosis was assessed by flow cytometry. Data were analyzed by 2-way ANOVA, interaction $p = 0.0016$. Significant comparisons by Bonferroni's multiple comparisons test are denoted on the graph. LB, Luria Broth.

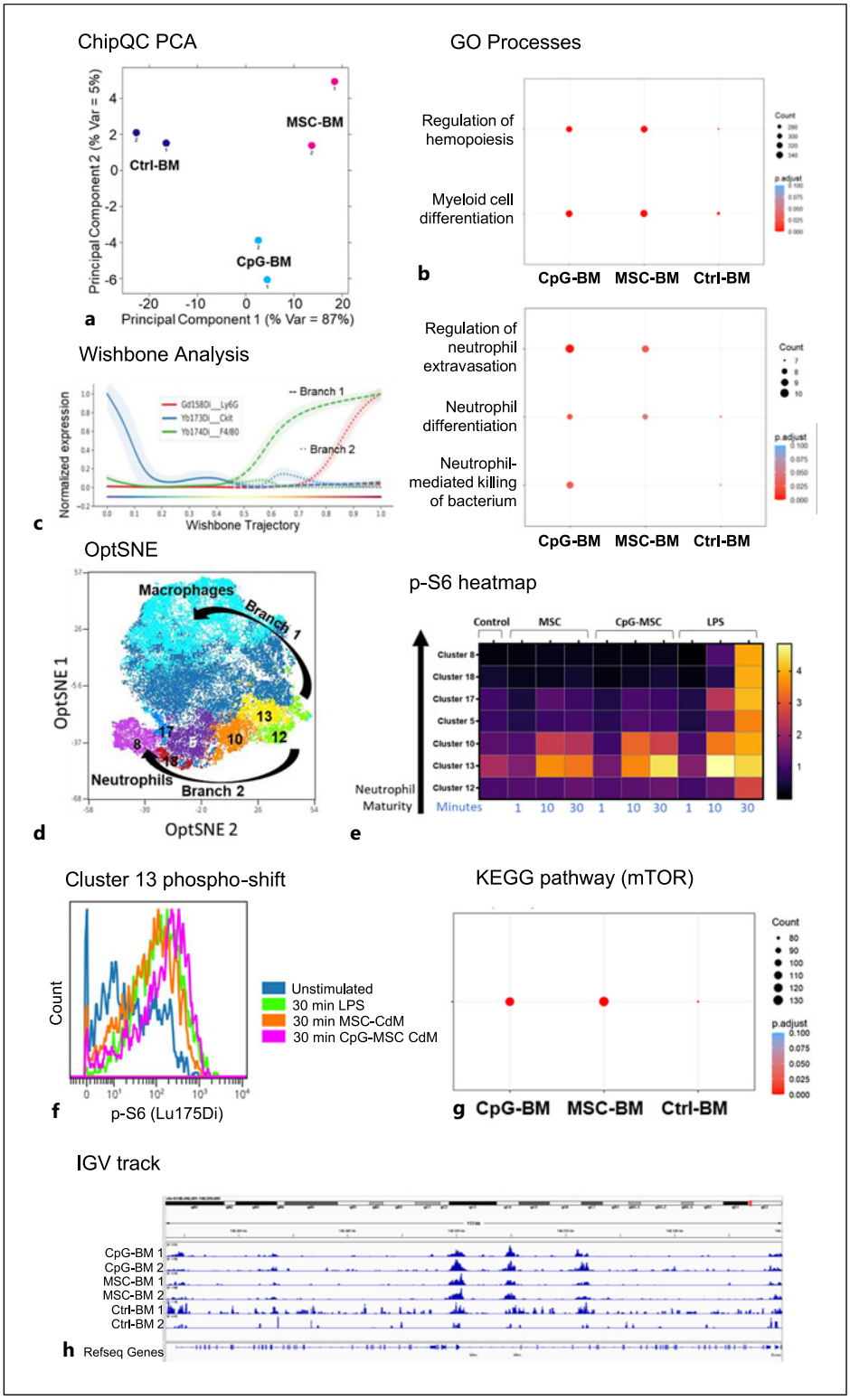

Fig. 2. C-kit+ hematopoietic stem cells from CpG-BM transplanted chimeric mice have persistent mTOR signaling and increased genes associated with myelopoiesis, and neutrophil function marked by H3K4me3. **a** Principal component analysis (PCA) of CUT&RUN data associated with H3K4me3 in c-kit+ cells from uninfected chimeras with Ctrl-BM (purple circles), MSC-BM (pink circles), or CpG-BM (blue circles) 16 weeks after transplantation. **b** Dot plot of functionally enriched gene ontology processes associated with myelopoiesis and neutrophil function in c-kit+ cells from chimeras. The number of genes in each gene set is represented by the size of each dot. The color of each dot indicates the significance of the pathway (adjusted *p* value) for each group. **c** Wishbone trajectory analysis of cells from the CAFC assay demonstrating a common c-kit+ trunk (blue solid line) and two distinct branches: (1) F4/80+ macrophages (green dashes, branch 1), and (2) Ly6G+ neutrophils (red dots, branch 2). **d** OptSNE plot demonstrating distinct clusters along the neutrophil fate trajectory. **e** Heatmap of relative p-S6 signaling (mTOR) after 1, 10, or 20 min of stimulation with medial control, MSC-CdM, CpG-MSC-CdM, or LPS in clusters along the neutrophil developmental pathway. **f** Representative shift in phospho-S6 (p-S6) signaling in cluster 13 30 min after stimulation with lipopolysaccharide (LPS, green), MSC-CdM (orange), or CpG-MSC-CdM (pink) compared to unstimulated control (blue). **g** Mechanistic target of rapamycin (mTOR) KEGG pathway overrepresentation analysis of chromatin associated with H3K4me3 in c-kit+ cells from chimeras. **h** Integrative genomic viewer (IGV) tracks of H3K4me3 peaks mTOR.

J Innate Immun 2023;15:765–781
DOI: 10.1159/000533732

Whole-genome analysis of H3K4me3-associated chromatin demonstrated distinct clustering between our chimera groups (Fig. 2a) by principal component analysis. We then sought to determine if there was enrichment of myelopoiesis and neutrophil-associated functional gene programs using the clusterProfiler [42] R package overrepresentation analysis [60] (Fig. 2b). While c-kit+ cells from chimeras transplanted with Ctrl-BM, MSC-BM, and CpG-BM all had significant H3K4me3 marks enriched in gene programs associated with the regulation of hemopoiesis and myeloid cell differentiation, there were more genes associated with each gene program in the c-kit+ cells from chimeras transplanted with MSC-BM and CpG-BM compared to Ctrl-BM (online suppl. Table 2). However, there was no major difference between chimeras transplanted with MSC-BM and CpG-BM. Given that c-kit+ HSCs are a heterogenous population comprising cells with both long-term and short-term repopulation and differentiation potential [61], it is expected that some c-kit+ cells isolated from chimeras transplanted with Ctrl-BM will be a more lineage-biased HSC subset that can readily respond to infection. Yet, c-kit+ cells isolated from chimeras transplanted with MSC-BM and CpG-BM have more genes associated with myelopoiesis and hemopoiesis marked by H3K4me3, suggesting that these cells are poised to more rapidly enhance emergency granulopoiesis responses, which is what was observed after infection of our chimeras. Evaluation of neutrophil-associated gene programs revealed that c-kit+ cells from chimeras transplanted with CpG-BM had enrichment of pathways involved in the regulation of neutrophil extravasation, neutrophil differentiation, and neutrophil-mediated killing of bacterium compared to chimeras transplanted with MSC-BM and Ctrl-BM, consistent with our in vitro functional data.

To identify mechanisms that may contribute to these HSC changes, we investigated the role of key signaling pathways by signaling cytometry by time of flight (CyTOF). Utilizing the CAFC assay (Fig. 1j), we stimulated the culture when cobblestone-forming areas were visualized with either lipopolysaccharide (positive control for visualization of phosphorylation shifts), alpha-MEM media control, MSC-CdM, or CpG-MSC-CdM for 1, 10, or 30 min. The cells were then labeled with phenotyping and phospho-signaling markers (online suppl. Table 3), and dimensionality reduction of CyTOF staining data was performed using optSNE. Clustering was performed using weighted PARC, which identified 20 independent clusters (online suppl. Fig. 3A). To get a sense of the relative significance of different signaling pathways after stimulation, we first plotted global changes in phosphorylation among all cells (online suppl. Fig. 3B), which demonstrated a strong phosphorylation shift in S6 after 10 and 30 min of stimulation with MSC- and CpG-MSC-CdM compared to control. We then sought to better define the cell population(s) exhibiting this shift. Given that all the stages of myeloid cell development (from c-kit+ stem cells to Ly6G+ neutrophils or F4/80+ macrophages) are encompassed within the CAFC assay, bifurcating cell fate trajectories were mapped from a randomly selected c-kit+ cell to identify distinct clusters along the developmental pathways to mature neutrophils or macrophages using the Wishbone algorithm [33] (Fig. 2c). This identified a trajectory defined in its early course by high c-kit+ expression (blue line) and low Ly6G (red line) and F/480 (green line) expression, followed by a transition to two clear branching points delineating the developmental pathways to a mature macrophage (branch 1, dashed line) or to a mature neutrophil (branch 2, dotted line). We then identified clusters that fell along the neutrophil developmental pathway (Fig. 2d) and created a heatmap representing the median expression of phospho-S6 along clusters defining the neutrophil developmental pathway (Fig. 2e). This identified significant phosphorylation shifts in S6, a marker of mechanistic target of rapamycin (mTOR) activity [62], after 10 and 30 min of stimulation with MSC- and CpG-MSC-CdM in cluster 10 and cluster 13 (Fig. 2f). This suggests that CdM acts primarily on an early, but not the most primitive, HSC, which expresses moderate, but not high, levels of c-kit, and PU.1, a transcription factor that instructs differentiation along the myeloid lineage [63] (online suppl. Fig. 3C).

To validate the significance of this signaling pathway, we performed an overrepresentation analysis of the genes associated with mTOR signaling marked by H3K4me3 in the c-kit+ cells from our chimeras using the KEGG pathway database (Fig. 2g). This demonstrated twice as many genes associated with the mTOR signaling pathway in chimeras transplanted with MSC-BM and CpG-BM compared to Ctrl-BM (online suppl. Table 2), with distinct peak differences observed in the integrative genomics viewer tracks (Fig. 2h). Taken together, the data suggest that mTOR signaling and the persistence of H3K4me3 marks associated with mTOR pathway genes may be involved in the enhanced myelopoietic potential of c-kit+ cells trained with MSC- and CpG-MSC-CdM.

CdM Enhances Emergency Granulopoiesis through Soluble Proteins

CdM from MSCs consist of soluble proteins (cytokines, chemokines, growth factors) and membranous cell-secreted vesicles called EV, which carry lipids, nucleic acids, and proteins. To determine whether EVs and/or soluble proteins are involved in augmenting emergency granulopoiesis, we first separated the CdM from MSCs and CpG-MSCs into an EV fraction, and an EVFSF using ultra-centrifugation (Fig. 3a), the gold standard for the isolation of EVs [29, 64, 65]. EVs were characterized as outlined by the International Society for Extracellular Vesicles [28] prior to use, including Western blot for CD81, CD9, and CD63 (Fig. 3b), nanoparticle tracking analysis to confirm that EVs are within an acceptable size range (Fig. 3c), and visualization by electron microscopy (Fig. 3d). There were no significant differences in the size or concentration of EVs found in MSC- versus CpG-MSC-CdM. To test the efficacy of these different fractions in augmenting emergency granulopoiesis, we used our previously published experimental model [14] (Fig. 3e), whereby mice are sublethally irradiated with 5 Gy radiation on day 0, injected retro-orbitally with media control, MSC- or CpG-MSC-CdM, MSC or CpG-MSC EVFSF, or MSC or CpG-MSC EVs on day 3, and infected with *P. aeruginosa* 7 days after radiation. Mice were sacrificed 2 days after infection and c-kit+ cells were isolated to perform colony-forming assays. Mice given MSC-CdM had more CFU-GMs (black bars) compared to media control (Fig. 3f). There was an equivalent increase in myeloid differentiation and proliferation potential as measured by CFU-GMs when mice were given the MSC EVFSF alone, although this was not observed when mice were given only MSC EVs. In contrast, there was an equivalent increase in CFU-GMs (Fig. 3g) when mice were given either complete CpG-MSC-CdM, the CpG-MSC EVFSF, or CpG-MSC EVs alone. This suggests that factors in the EVFSF [66] are driving the observed effect in CdM from both MSCs and CpG-MSCs, while EVs in CpG-MSC-CdM also contribute to the increase in myeloid cell differentiation.

Calreticulin in the CdM May Mediate Neutrophil-Trained Immunity as a Part of a Protein Complex

Given that soluble protein(s) might mediate the observed effect, we performed protein mass spectrometry on the MSC and CpG-MSC secretomes to identify potential protein/protein complex targets for evaluation as a first step in identifying factors that mediate neutrophil-trained immunity. A total of 3,729 peptides and 772 proteins were quantified between all submitted samples. Principal component analysis of the two secretomes demonstrated separation of the two samples along principal component 1 (Fig. 4a), accounting for 26.2% of the variance. Using a cutoff of $p < 0.01$ and fold change >2, we identified 31 proteins that were upregulated in the CpG-MSC secretome relative to the MSC secretome (Fig. 4b and online supplementary Table 4). As proteins often function in complexes and interact with each other to carry out biological processes, we constructed a physical protein-protein interaction network from the top 15 upregulated proteins in the CpG-MSC secretome (Fig. 4c) using the STRING database [45].This identified two potential physical protein complexes, including one with calreticulin as a central "hub" (a protein with many interactions representing a protein of critical importance to a biological process). Calreticulin is a multifunctional soluble protein with critical roles in myeloproliferative disorders [67] and macrophage activation [68], suggesting it can have pleiotropic effects on myelopoiesis and innate immune function.

To investigate the role of calreticulin in enhancing myelopoiesis, lineage-negative c-kit+ HSCs were isolated from Balb/cByJ mice and cultured in StemSpan SFEM II with media control, MSC-CdM, CpG-MSC-CdM, or 10 ng of calreticulin (Millipore Sigma, Cat SRP8001) for 48 h. C-kit+ cells from equal volume aliquots from each culture condition were plated and cultured in methylcellulose for 14 days and colonies were quantified. Using MSC- and CpG-MSC-CdM, we demonstrated that this in vitro myelopoiesis assay recapitulated our prior observations (Fig. 4d), showing that c-kit+ cells stimulated with MSC- or CpG-MSC-CdM had increased myeloid proliferation and differentiation potential, compared to media control. When we stimulated lineage-negative c-kit+ HSCs with calreticulin, there was no statistically significant increase in the number of c-kit+ cells in culture (Fig. 4e) or CFU (Fig. 4f) after 2 weeks in culture. However, we did note a significant increase in the total number of cells per CFU plate, suggesting that more myeloid cells are generated from a single c-kit+ HSC after stimulation with calreticulin, compared to media control. This suggests that calreticulin may increase the myelopoiesis potential of a given HSC without increasing the total pool of HSCs, a critical function in response to infection.

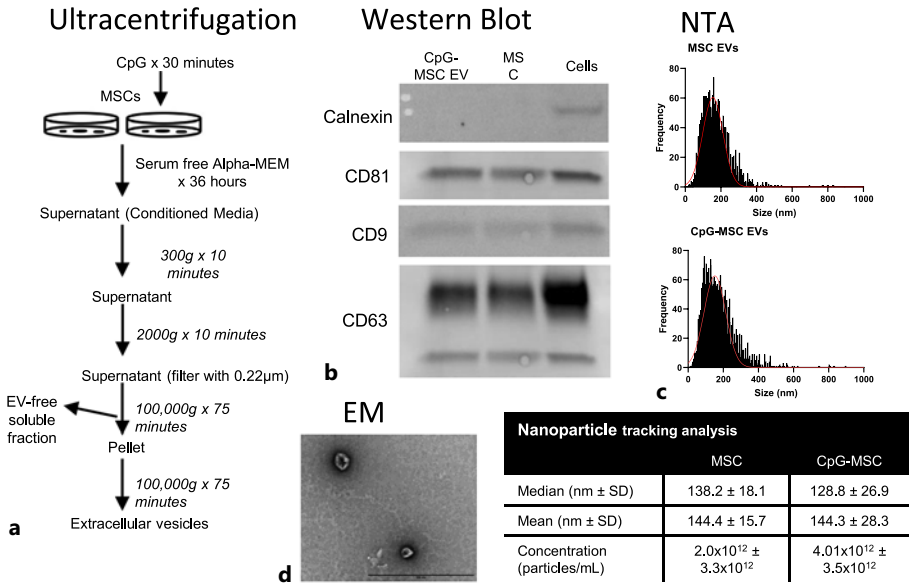

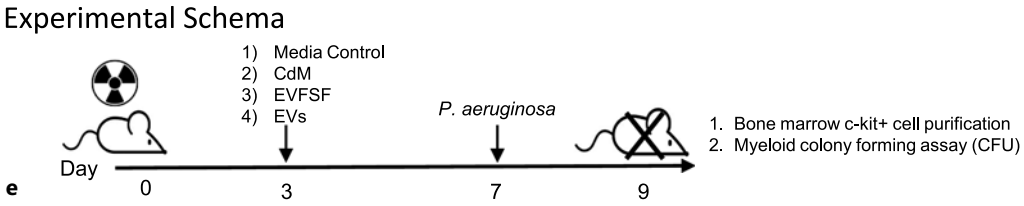

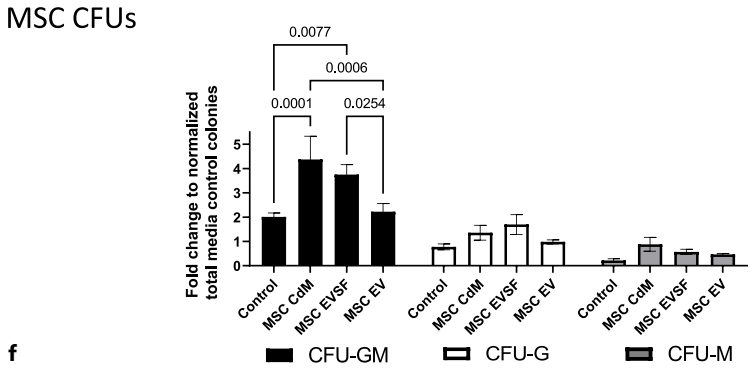

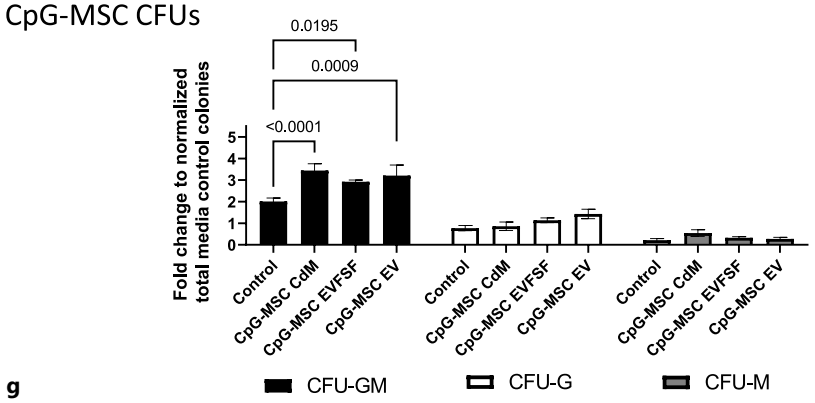

3

(For legend see next page.)

Discussion

In this paper, we demonstrated that paracrine factors secreted by MSCs can leave H3K4me3 marks in lineage-negative c-kit+ HSCs at genes associated with myelopoiesis, leaving them "poised" to enhance emergency granulopoiesis in response to a subsequent bacterial infection. When MSCs are preconditioned with CpG, there is a small but additive effect of further enhancing neutrophil function.

Currently, BCG and β-glucan, a component of the fungal cell wall, are two of the most well-described mediators of trained immunity, and there is a robust body of work demonstrating memory features in monocytes and macrophages [56, 69]. Within this growing body of literature, however, trained immunity in neutrophil progenitor cells remain sparsely studied. In humans, BCG vaccination produces a myeloid-skewed gene signature in progenitor populations and activation of neutrophil-mediated gene programs [70]. Furthermore, BCG vaccination can enhance neutrophil phagocytosis and the production of reactive oxygen species [53], while β-glucan can train HSCs to enhance granulopoiesis [71, 72]. Trained immunity has been described at the level of hematopoietic stem and progenitor cells, both in the context of infections [73], as well as chronic inflammatory diseases [74, 75], but typically as a result of direct training. Others have shown that MSC-derived EVs can ameliorate murine neonatal lung injury by epigenetically reprogramming monocytes [76]; however, its role in training HSCs has not been explored.

In this paper, we sought to expand on our previously published data on the protective role of paracrine factors from CpG-MSCs in sepsis [14] to elucidate the mechanisms underlying this observed effect. Using a chimera model, we first demonstrated that CpG-MSC-CdM act specifically on lineage-negative c-kit+ HSCs to enhance emergency granulopoiesis and neutrophil function in response to a subsequent infection. However, this phenotype is only observed in the context of infection; uninfected chimeras had similar peripheral blood immune cell populations and plasma cytokines, suggesting that the HSCs are being trained rather than primed, the former being defined by a return to a basal functional state [47]. This study represents the first to demonstrate that paracrine factors from MSCs can act as novel mediators of neutrophil-trained immunity in lineage-negative c-kit+ HSCs.

Histone modifications by specific epigenetic enzymes such as histone methyltransferases and acetylases are well-described regulators of the inflammatory gene programs involved in the host response to infection [77]. In trained cells, shifts in cellular metabolism have been shown to change the availability of metabolites that can act as substrates for these epigenetic enzymes, activating or repressing their function, and thereby changing the epigenetic landscape [78]. In monocytes, mevalonate, a component of the cholesterol synthesis pathway, activates insulin-like growth factor-1 receptor and mTOR that leads to epigenetic changes in inflammatory pathways [79]. Trained monocytes also demonstrate increased glycolysis that is dependent on activation of mTOR through a dectin-1/Akt/HIF1α pathway [56]. Furthermore, these changes in metabolic pathways have been demonstrated in myeloid progenitors in the bone marrow, suggesting that these longer lived populations may be key in mediating the longevity of this trained effect [71]. These preexisting studies on the mechanisms of trained immunity lend strong support to our data. In this study, we demonstrated that paracrine factors from MSCs with and without CpG preconditioning can leave H3K4me3

Fig. 3. Both the EVFSF and EVs in CdM from CpG-MSCs augment emergency granulopoiesis. **a** Ultra-centrifugation protocol for the preparation of EV and the EVFSF from the same starting CdM. **b** The EV fraction from MSCs and CpG-MSCs were analyzed by Western blot for calnexin (negative control), CD81, CD9, and CD63, with whole cell protein as positive control. **c** Nanoparticle tracking analysis (NTA) of EV characteristics and size distribution of MSC EVs and CpG-MSC EVs. **d** Transmission electron microscopy image demonstrating CpG-MSC EV morphology. Scale bar represents 100 nm. **e** Schematic of experimental model. Mice received a sublethal dose of irradiation (5 Gy) on day 0. On day 3, mice were given 150 μL of either (1) alpha-MEM media control, (2) CdM from 5×10^5 MSC or CpG-MSCs, (3) EV-free soluble fraction (EVFSF) from 5×10^5 MSC or CpG-MSCs, or (4) EVs from 5×10^5 MSCs or CpG-MSCs. On day 7, mice were infected intranasally with *P. aeruginosa*, and sacrificed 2 days after infection to isolate c-kit+ cells for a myeloid colon-forming assay. **f** Myeloid differentiation and proliferation potential of c-kit+ cells ($n = 6$ per group) from infected and irradiated mice given MSC-CdM, MSC EVSF, MSC EVs, or media control as measured by CFU-GM (black bar), CFU-G (white bar), and CFU-M (gray bar). Data were analyzed by 2-way ANOVA, interaction $p = 0.0714$, row factor $p = 0.0002$. **g** Myeloid differentiation and proliferation potential of c-kit+ cells ($n = 6$ per group) from infected and irradiated mice given CpG-MSC-CdM, CpG-MSC EVSF, CpG-MSC EVs, or media control. Data were analyzed by 2-way ANOVA, interaction $p = 0.0214$. **f**, **g** Significant comparisons by Bonferroni's multiple comparisons test are denoted on the graphs.

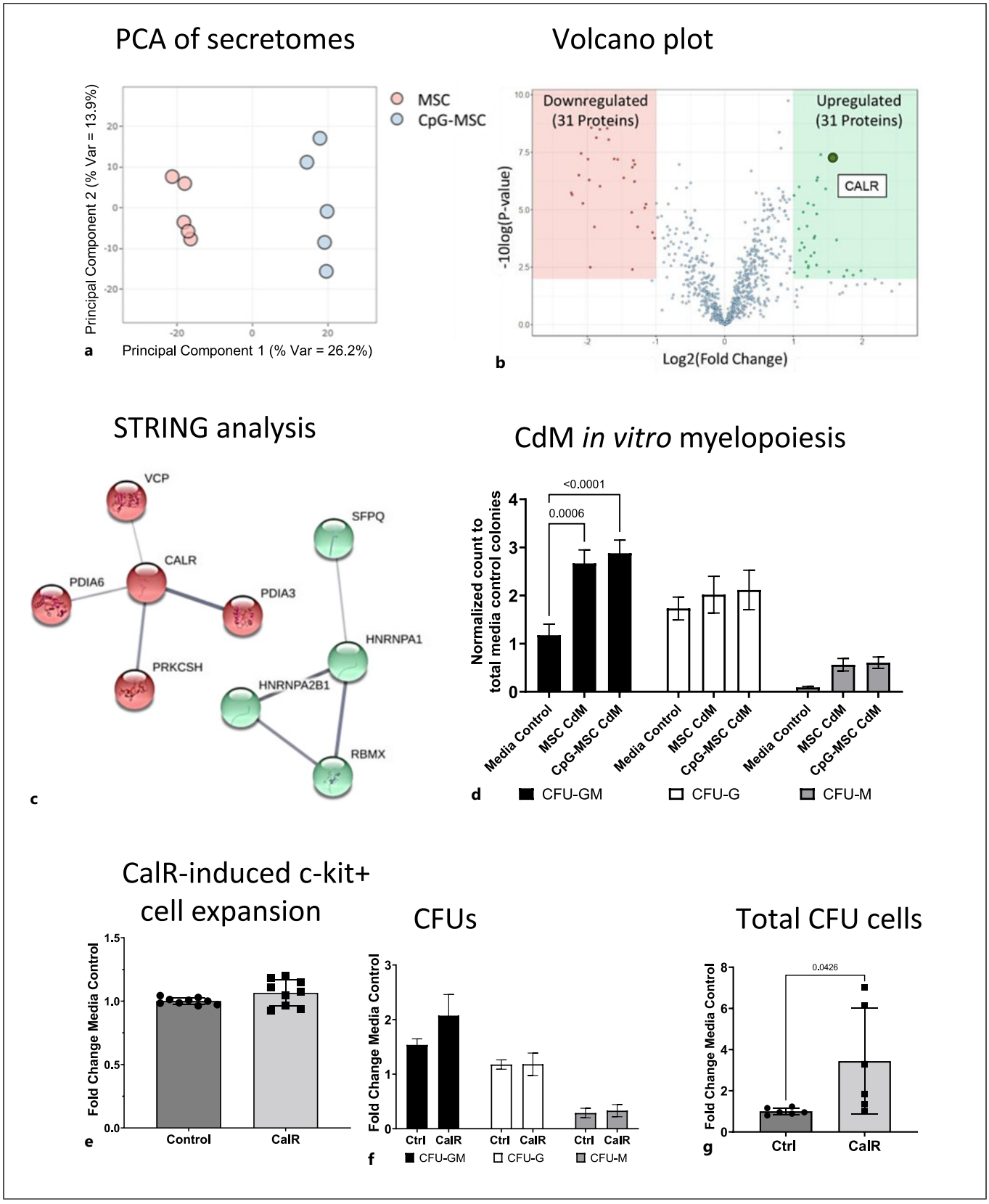

4

(For legend see next page.)

histone marks at the promoters and 5' untranslated regions of genes associated with the regulation of hemopoiesis and myeloid cell differentiation. We additionally demonstrated that soluble factors in the CdM strongly activated the mTOR pathway in HSCs in vitro, a pathway that remained highly marked by H3K4me4 modifications in our chimeric mice compared to control. Interestingly, our in vitro data demonstrated the strongest phospho-S6 signal in an early neutrophil progenitor cell after stimulation with CdM, representing one of the few studies to identify the specific population of HSCs that can be trained. Taken together, this suggests that MSCs, an integral part of the hematopoietic niche, can secrete paracrine factors and may alter the glycolysis metabolism of HSCs, leaving early progenitor cells poised to differentiate into myeloid cells and enhance neutrophil function in response to infection. Further investigation utilizing single cell technology in lineage-negative, c-kit+ cells from our chimeras may yield additional insight into these populations and associated metabolic pathways in vivo.

Preclinical studies have demonstrated that CdM alone has an effect size comparable to whole cell therapy [80], and that both soluble proteins [81] and EV can restore stem cell engraftment postirradiation [82]. Due to the wealth of soluble factors secreted by MSCs with pleiotropic effects in different inflammatory microenvironments, the identification of key mediator(s) of biological processes in the CdM has been limited. In this paper, we begin to tease out these mediators by demonstrating that soluble proteins from MSCs can leave HSCs poised to enhance emergency myelopoiesis. This effect was observed with EVs alone when they were derived from CpG-MSCs, but not from unconditioned MSCs. This suggests that the small additive effect of further enhancing trained immunity by preconditioning MSCs with CpG may be derived from CpG-MSC EVs. Intriguingly proteomic analysis of the CpG-MSC compared to the MSC secretome demonstrated an almost 3-fold upregulation of calreticulin, a protein that has been previously described in the MSC secretome [83, 84]. The role of mutant calreticulin in myeloproliferative neoplasms is well described [85], although its functions as an extracellular immunomodulatory protein and its role in steady-state hematopoiesis are burgeoning fields. For example, secreted calreticulin can act as an "eat me" signal and activate macrophages [86] to facilitate programmed cell removal [68, 87]. Overexpression of wild-type calreticulin in human CD34+ stem cells can also enhance erythroid and megakaryocyte differentiation [88]. These studies lend evidence to the potential for calreticulin to act as an intermediary between hematopoiesis and the immune response. In our studies, extracellular calreticulin did not have an immediate effect on HSC proliferation or myeloid colony numbers but may have a delayed effect related to enhanced myelopoiesis by increasing the number of cells derived from a single c-kit+ HSC. Future studies to investigate role in trained immunity are warranted.

Currently, advances in cancer care have improved disease-free and overall survival rates, but their utility are often limited by life-threatening pulmonary infections [4, 5]. The functional reprogramming of innate immune cells to enhance the host response against a broad range of subsequent infections – trained immunity – is a promising paradigm for reducing this burden of disease [19, 22, 89]. Here, we present data demonstrating soluble proteins from MSCs as novel mediators of neutrophil-trained immunity, representing a new prophylactic strategy for reducing the burden of disease from severe respiratory infections.

Fig. 4. Proteomic analysis of CpG-MSC- and MSC-CdM identifies soluble calreticulin as a mediator of neutrophil-trained immunity. **a** Principal component analysis (PCA) of MSC (pink, $n = 5$) and CpG-MSC (blue, $n = 5$) protein secretomes. **b** Volcano plot demonstrating up-(green) and down-(red) regulated proteins from CpG-MSC-CdM compared to MSC-CdM ($p < 0.01$, fold change >2). The complete list of proteins identified as significant are listed in online supplementary Table 4. **c** STRING analysis of 9 of the top 15 upregulated proteins demonstrating two physical subnetworks, where the nodes indicate proteins and the edges indicate physical interactions that have been described by text mining of experiments or databases. The thickness of the edge indicates the strength of the data support. Protein-protein interaction (PPI) enrichment p value = $5.76e^{-06}$. CALR, calreticulin; HNRNPA1, heterogenous nuclear ribonucleoprotein A1; HNRNP2B1, heterogenous nuclear ribonucleoproteins A2/B1; PDIA3, protein disulfide-isomerase A3; PDIA6, protein disulfide-isomerase A6; PRKCSH, protein kinase c substrate 80k–h; SFPQ, splicing factor, proline- and glutamine-rich; RBMX, heterogenous nuclear ribonucleoprotein g; VCP, transitional endoplasmic reticulum ATPase. **d** Myeloid differentiation and proliferation potential of lineage-negative c-kit+ HSCs cultured in StemSpan and 20% media control, MSC-CdM, or CpG-MSC-CdM for 48 h ($n = 6$ per group). Data were analyzed by 2-way ANOVA, interaction $p = 0.0675$, row factor $p = 0.0003$. Significant comparisons by Bonferroni's multiple comparisons tests were performed and denoted on the graph. **e** The number of lineage-negative, c-kit+ hematopoietic stem cells in vitro after 48 h stimulation with media control or calreticulin. Data were analyzed by unpaired t test, $p = 0.0848$. **f** C-kit+ cells were cultured in methylcellulose and colonies were quantified. Data were analyzed by 2-way ANOVA, interaction $p = 0.7046$. **g** Total cells from the colony-forming assay plate were quantified by flow cytometry. Data were analyzed by unpaired t test, $p = 0.0426$.

Acknowledgments

Electron microscopy imaging, consultation, and service were performed in the Harvard Medical School Electron Microscopy facility. Next-generation sequencing consultation and services were provided by the Molecular Biology Core Facilities at Dana-Farber Cancer Institute. Proteomic services were performed at the Thermo Fisher Scientific Center for Multiplexed Proteomics at Harvard Medical School (http://tcmp.hms.edu).

Statement of Ethics

All mouse experiments performed in this study were approved by the Animal Care and Use Committee at Brigham and Women's Hospital (IACUC Protocol 2020N000053). The Brigham and Women's Hospital IACUC follows the international ARRIVE guidelines.

Conflict of Interest Statement

The authors have no conflicts of interest to declare.

Funding Sources

This research was supported by the following funding sources, all from the National Institutes of Health (NIH): T32HL007633-30, U01AI138318, R01GM136804, R01AI148232, P30AR070253.

Author Contributions

Julie Ng participated in the experimental design, carried out most of the experiments, and drafted the manuscript. Anna Marneth participated in the generation of chimeric mice. Alec Griffith carried out the signaling CyTOF experiments. Yang Shi and Alan Jiao advised us and helped with CUT&RUN analysis. Gareth Willis performed the nanoparticle tracking analysis and Junwen Han helped with experiments involving EVs. Jewel Imani and Daniel Younger helped with bone marrow transplantation. Sailaja Ghanta, Junwen Han, and Bailin Niu helped with the human MSC culturing work. Daniel Younger, Sailaja Ghanta, Brandon Hancock, Fei Guo, and Joshua Keegan helped with the in vivo experiments. Mark Perrella and James Lederer participated in the conception, design, and coordination of the study. All authors have read and approved the final manuscript.

Data Availability Statement

Data that support the interpretation of findings presented in this paper are openly available. All CUT&RUN sequencing data reported in this study are available at GEO GSE199338. Additional analysis files and scripts are available upon request. Interactive proteomics data can be found at: http://caribou.med.harvard.edu/tmtviewer/?sessid=ZSTAF9655P62OZXKM2F40GPMW46314QDN. CyTOF staining data generated in this study will be shared on ImmPort.org at the time of publication. Further inquiries can be directed to the corresponding author.

References

1 GBD 2016 Lower Respiratory Infections Collaborators. Estimates of the global, regional, and national morbidity, mortality, and aetiologies of lower respiratory infections in 195 countries, 1990-2016: a systematic analysis for the Global Burden of Disease Study 2016. Lancet Infect Dis. 2018 Nov;18(11):1191–210.
2 Tong S, Amand C, Kieffer A, Kyaw MH. Trends in healthcare utilization and costs associated with pneumonia in the United States during 2008-2014. BMC Health Serv Res. 2018 Sep 14;18(1):715.
3 Storms AD, Chen J, Jackson LA, Nordin JD, Naleway AL, Glanz JM, et al. Rates and risk factors associated with hospitalization for pneumonia with ICU admission among adults. BMC Pulm Med. 2017 Dec 16;17(1):208.
4 Brenner H, Gondos A, Arndt V. Recent major progress in long-term cancer patient survival disclosed by modeled period analysis. J Clin Oncol. 2007 Aug 1;25(22):3274–80.
5 Gohil A, Khazeni N. Diagnostic strategy for hematology and oncology patients with acute respiratory failure. Am J Respir Crit Care Med. 2011 Jan 15;183(2):279; author reply 279-80.
6 Lossos IS, Breuer R, Or R, Strauss N, Elishoov H, Naparstek E, et al. Bacterial pneumonia in recipients of bone marrow transplantation. A five-year prospective study. Transplantation. 1995 Oct 15;60(7):672–8.
7 Huynh TN, Weigt SS, Belperio JA, Territo M, Keane MP. Outcome and prognostic indicators of patients with hematopoietic stem cell transplants admitted to the intensive care unit. J Transpl. 2009;2009:917294.
8 Michel CS, Teschner D, Schmidtmann I, Theobald M, Hauptrock B, Wagner-Drouet EM, et al. Prognostic factors and outcome of adult allogeneic hematopoietic stem cell transplantation patients admitted to intensive care unit during transplant hospitalization. Sci Rep. 2019 Dec 27;9(1):19911.
9 Nelson RE, Hatfield KM, Wolford H, Samore MH, Scott RD, Reddy SC, et al. National estimates of healthcare costs associated with multidrug-resistant bacterial infections among hospitalized patients in the United States. Clin Infect Dis. 2021;72(Suppl 1):S17–26.
10 Dominici M, Le Blanc K, Mueller I, Slaper-Cortenbach I, Marini F, Krause D, et al. Minimal criteria for defining multipotent mesenchymal stromal cells. The International Society for Cellular Therapy position statement. Cytotherapy. 2006;8(4):315–7.
11 Goloviznina NA, Verghese SC, Yoon YM, Taratula O, Marks DL, Kurre P. Mesenchymal stromal cell-derived extracellular vesicles promote myeloid-biased multipotent hematopoietic progenitor expansion via Toll-like receptor engagement. J Biol Chem. 2017 Feb 24;292(8):3541.
12 Shi C, Jia T, Mendez-Ferrer S, Hohl TM, Serbina NV, Lipuma L, et al. Bone marrow mesenchymal stem and progenitor cells induce monocyte emigration in response to circulating toll-like receptor ligands. Immunity. 2011 Apr 22;34(4):590–601.
13 Hall SR, Tsoyi K, Ith B, Padera RF Jr, Lederer JA, Wang Z, et al. Mesenchymal stromal cells improve survival during sepsis in the absence of heme oxygenase-1: the importance of neutrophils. Stem Cell. 2013 Feb;31(2):397–407.
14 Ng J, Guo F, Marneth AE, Ghanta S, Kwon MY, Keegan J, et al. Augmenting emergency granulopoiesis with CpG conditioned mesenchymal stromal cells in murine neutropenic sepsis. Blood Adv. 2020 Oct 13;4(19):4965–79.

15 Manz MG, Boettcher S. Emergency granulopoiesis. Nat Rev Immunol. 2014 May; 14(5):302–14.
16 Aaby P, Roth A, Ravn H, Napirna BM, Rodrigues A, Lisse IM, et al. Randomized trial of BCG vaccination at birth to low-birth-weight children: beneficial nonspecific effects in the neonatal period? J Infect Dis. 2011 Jul 15; 204(2):245–52.
17 de Castro MJ, Pardo-Seco J, Martinón-Torres F. Nonspecific (heterologous) protection of neonatal BCG vaccination against hospitalization due to respiratory infection and sepsis. Clin Infect Dis. 2015 Jun 1; 60(11):1611–9.
18 Bawankule R, Singh A, Kumar K, Shetye S. Does measles vaccination reduce the risk of acute respiratory infection (ARI) and diarrhea in children: a multi-country study? PLoS One. 2017;12(1):e0169713.
19 Netea MG, Quintin J, van der Meer JW. Trained immunity: a memory for innate host defense. Cell Host Microbe. 2011 May 19; 9(5):355–61.
20 Mauer AM, Athens JW, Ashenbrucker H, Cartwright GE, Wintrobe MM. Leukokinetic studies. II. A method for labeling granulocytes in vitro with radioactive DIIsopropylfluorophosphate (dfp). J Clin Invest. 1960 Sep;39(9):1481–6.
21 Patel AA, Zhang Y, Fullerton JN, Boelen L, Rongvaux A, Maini AA, et al. The fate and lifespan of human monocyte subsets in steady state and systemic inflammation. J Exp Med. 2017 Jul 3;214(7):1913–23.
22 Netea MG, Domínguez-Andrés J, Barreiro LB, Chavakis T, Divangahi M, Fuchs E, et al. Defining trained immunity and its role in health and disease. Nat Rev Immunol. 2020 Jun;20(6):375–88.
23 Miao R, Lim VY, Kothapalli N, Ma Y, Fossati J, Zehentmeier S, et al. Hematopoietic stem cell niches and signals controlling immune cell development and maintenance of immunological memory. Front Immunol. 2020; 11:600127.
24 Zhang J, Wu Q, Johnson CB, Pham G, Kinder JM, Olsson A, et al. In situ mapping identifies distinct vascular niches for myelopoiesis. Nature. 2021;590(7846):457–62.
25 Schneider RK, Mullally A, Dugourd A, Peisker F, Hoogenboezem R, Van Strien PMH, et al. Gli1(+) mesenchymal stromal cells are a key driver of bone marrow fibrosis and an important cellular therapeutic target. Cell Stem Cell. 2017 Jun 1; 20(6):785–800.e8.
26 de Haan G, Ploemacher R. The cobblestone-area-forming cell assay. Methods Mol Med. 2002;63:143–51.
27 Han J, Shi Y, Willis G, Imani J, Kwon MY, Li G, et al. Mesenchymal stromal cell-derived syndecan-2 regulates the immune response during sepsis to foster bacterial clearance and resolution of inflammation. Febs j. 2022; 289(2):417–35.
28 Thery C, Witwer KW, Aikawa E, Alcaraz MJ, Anderson JD, Andriantsitohaina R, et al. Minimal information for studies of extracellular vesicles 2018 (MISEV2018): a position statement of the International Society for Extracellular Vesicles and update of the MISEV2014 guidelines. J Extracell Vesicles. 2018;7(1):1535750.
29 Willis GR, Fernandez-Gonzalez A, Anastas J, Vitali SH, Liu X, Ericsson M, et al. Mesenchymal stromal cell exosomes ameliorate experimental bronchopulmonary dysplasia and restore lung function through macrophage immunomodulation. Am J Respir Crit Care Med. 2018 Jan 1;197(1):104–16.
30 Zunder ER, Finck R, Behbehani GK, Amir EAD, Krishnaswamy S, Gonzalez VD, et al. Palladium-based mass tag cell barcoding with a doublet-filtering scheme and single-cell deconvolution algorithm. Nat Protoc. 2015 Feb;10(2):316–33.
31 Finck R, Simonds EF, Jager A, Krishnaswamy S, Sachs K, Fantl W, et al. Normalization of mass cytometry data with bead standards. Cytometry A. 2013 May;83(5):483–94.
32 Stassen SV, Siu DMD, Lee KCM, Ho JWK, So HKH, Tsia KK. PARC: ultrafast and accurate clustering of phenotypic data of millions of single cells. Bioinformatics. 2020;36(9):2778–86.
33 Setty M, Tadmor MD, Reich-Zeliger S, Angel O, Salame TM, Kathail P, et al. Wishbone identifies bifurcating developmental trajectories from single-cell data. Nat Biotechnol. 2016 Jun;34(6):637–45.
34 Langmead B, Salzberg SL. Fast gapped-read alignment with Bowtie 2. Nat Methods. 2012 Mar 4;9(4):357–9.
35 Ramírez F, Ryan DP, Grüning B, Bhardwaj V, Kilpert F, Richter AS, et al. deepTools2: a next generation web server for deep-sequencing data analysis. Nucleic Acids Res. 2016 Jul 8; 44(W1):W160–5.
36 Carroll TS, Liang Z, Salama R, Stark R, de Santiago I. Impact of artifact removal on ChIP quality metrics in ChIP-seq and ChIP-exo data. Front Genet. 2014;5:75.
37 Zhang Y, Liu T, Meyer CA, Eeckhoute J, Johnson DS, Bernstein BE, et al. Model-based analysis of ChIP-seq (MACS). Genome Biol. 2008;9(9):R137.
38 Li Q, Brown JB, Huang H, Bickel PJ. Measuring reproducibility of high-throughput experiments. Ann Appl Stat. 2011;5(3):1752–79.
39 Quinlan AR, Hall IM. BEDTools: a flexible suite of utilities for comparing genomic features. Bioinformatics. 2010;26(6):841–2.
40 Yu G, Wang L-G, He Q-Y. ChIPseeker: an R/Bioconductor package for ChIP peak annotation, comparison and visualization. Bioinformatics. 2015;31(14):2382–3.
41 Yu G, Wang LG, Han Y, He QY. clusterProfiler: an R package for comparing biological themes among gene clusters. Omics. 2012 May;16(5):284–7.
42 Wu T, Hu E, Xu S, Chen M, Guo P, Dai Z, et al. clusterProfiler 4.0: a universal enrichment tool for interpreting omics data. Innovation. 2021;2(3):100141.
43 Navarrete-Perea J, Yu Q, Gygi SP, Paulo JA. Streamlined tandem mass tag (SL-TMT) protocol: an efficient strategy for quantitative (Phospho)proteome profiling using tandem mass tag-synchronous precursor selection-MS3. J Proteome Res. 2018 Jun 1;17(6): 2226–36.
44 Eng JK, McCormack AL, Yates JR. An approach to correlate tandem mass spectral data of peptides with amino acid sequences in a protein database. J Am Soc Mass Spectrom. 1994 Nov;5(11):976–89.
45 Szklarczyk D, Gable AL, Lyon D, Junge A, Wyder S, Huerta-Cepas J, et al. STRING v11: protein-protein association networks with increased coverage, supporting functional discovery in genome-wide experimental datasets. Nucleic Acids Res. 2019 Jan 8;47(D1): D607–13.
46 Elf S, Abdelfattah NS, Chen E, Perales-Patón J, Rosen EA, Ko A, et al. Mutant calreticulin requires both its mutant C-terminus and the thrombopoietin receptor for oncogenic transformation. Cancer Discov. 2016;6(4):368–81.
47 Divangahi M, Aaby P, Khader SA, Barreiro LB, Bekkering S, Chavakis T, et al. Trained immunity, tolerance, priming and differentiation: distinct immunological processes. Nat Immunol. 2021 Jan;22(1):2–6.
48 Remick DG, Bolgos G, Copeland S, Siddiqui J. Role of interleukin-6 in mortality from and physiologic response to sepsis. Infect Immun. 2005;73(5):2751–7.
49 Morrow KN, Coopersmith CM, Ford ML. IL-17, IL-27, and IL-33: a novel Axis linked to immunological dysfunction during sepsis. Front Immunol. 2019;10:1982.
50 Amarachintha S, Pang Q. Cobblestone area-forming cell assay of mouse bone marrow hematopoietic stem cells. Bio Protoc. 2018 May 5;8(9):e2824.
51 Bird A. Perceptions of epigenetics. Nature. 2007 May 24;447(7143):396–8.
52 Saccani S, Pantano S, Natoli G. p38-Dependent marking of inflammatory genes for increased NF-kappa B recruitment. Nat Immunol. 2002 Jan;3(1):69–75.
53 Moorlag S, Rodriguez-Rosales YA, Gillard J, Fanucchi S, Theunissen K, Novakovic B, et al. BCG vaccination induces long-term functional reprogramming of human neutrophils. Cell Rep. 2020 Nov 17;33(7):108387.
54 Creyghton MP, Cheng AW, Welstead GG, Kooistra T, Carey BW, Steine EJ, et al. Histone H3K27ac separates active from poised enhancers and predicts developmental state. Proc Natl Acad Sci U S A. 2010 Dec 14; 107(50):21931–6.
55 Quintin J, Saeed S, Martens JHA, Giamarellos-Bourboulis EJ, Ifrim DC, Logie C, et al. Candida albicans infection affords protection against reinfection via functional reprogramming of monocytes. Cell Host Microbe. 2012 Aug 16;12(2):223–32.

56 Cheng SC, Quintin J, Cramer RA, Shepardson KM, Saeed S, Kumar V, et al. mTOR- and HIF-1α-mediated aerobic glycolysis as metabolic basis for trained immunity. Science. 2014 Sep 26;345(6204):1250684.
57 Saeed S, Quintin J, Kerstens HH, Rao NA, Aghajanirefah A, Matarese F, et al. Epigenetic programming of monocyte-to-macrophage differentiation and trained innate immunity. Science. 2014 Sep 26;345(6204):1251086.
58 Hainer SJ, Fazzio TG. High-Resolution chromatin profiling using CUT&RUN. Curr Protoc Mol Biol. 2019 Apr;126(1):e85.
59 Landt SG, Marinov GK, Kundaje A, Kheradpour P, Pauli F, Batzoglou S, et al. ChIP-seq guidelines and practices of the ENCODE and modENCODE consortia. Genome Res. 2012 Sep;22(9):1813–31.
60 Boyle EI, Weng S, Gollub J, Jin H, Botstein D, Cherry JM, et al. GO-TermFinder: open source software for accessing Gene Ontology information and finding significantly enriched Gene Ontology terms associated with a list of genes. Bioinformatics. 2004 Dec 12;20(18):3710–5.
61 Jurecic R. Hematopoietic stem cell heterogeneity. Adv Exp Med Biol. 2019;1169:195–211.
62 Iwenofu OH, Lackman RD, Staddon AP, Goodwin DG, Haupt HM, Brooks JS. Phospho-S6 ribosomal protein: a potential new predictive sarcoma marker for targeted mTOR therapy. Mod Pathol. 2008 Mar;21(3):231–7.
63 Iwasaki H, Somoza C, Shigematsu H, Duprez EA, Iwasaki-Arai J, Mizuno SI, et al. Distinctive and indispensable roles of PU.1 in maintenance of hematopoietic stem cells and their differentiation. Blood. 2005;106(5):1590–600.
64 Momen-Heravi F, Balaj L, Alian S, Mantel PY, Halleck AE, Trachtenberg AJ, et al. Current methods for the isolation of extracellular vesicles. Biol Chem. 2013 Oct;394(10):1253–62.
65 Lane RE, Korbie D, Trau M, Hill MM. Purification protocols for extracellular vesicles. Methods Mol Biol. 2017;1660:111–30.
66 Brennan M, Layrolle P, Mooney DJ. Biomaterials functionalized with MSC secreted extracellular vesicles and soluble factors for tissue regeneration. Adv Funct Mater. 2020 Sep 10;30(37):30.
67 Klampfl T, Gisslinger H, Harutyunyan AS, Nivarthi H, Rumi E, Milosevic JD, et al. Somatic mutations of calreticulin in myeloproliferative neoplasms. N Engl J Med. 2013 Dec 19;369(25):2379–90.
68 Chao MP, Jaiswal S, Weissman-Tsukamoto R, Alizadeh AA, Gentles AJ, Volkmer J, et al. Calreticulin is the dominant pro-phagocytic signal on multiple human cancers and is counterbalanced by CD47. Sci Transl Med. 2010 Dec 22;2(63):63ra94.
69 Arts RJW, Moorlag S, Novakovic B, Li Y, Wang SY, Oosting M, et al. BCG vaccination protects against experimental viral infection in humans through the induction of cytokines associated with trained immunity. Cell Host Microbe. 2018 Jan 10;23(1):89–100.e5.
70 Cirovic B, de Bree LCJ, Groh L, Blok BA, Chan J, van der Velden W, et al. BCG vaccination in humans elicits trained immunity via the hematopoietic progenitor compartment. Cell Host Microbe. 2020 Aug 12;28(2):322–34.e5.
71 Mitroulis I, Ruppova K, Wang B, Chen LS, Grzybek M, Grinenko T, et al. Modulation of myelopoiesis progenitors is an integral component of trained immunity. Cell. 2018 Jan 11;172(1–2):147–61.e12.
72 Kalafati L, Kourtzelis I, Schulte-Schrepping J, Li X, Hatzioannou A, Grinenko T, et al. Innate immune training of granulopoiesis promotes anti-tumor activity. Cell. 2020 Oct 29;183(3):771–85.e12.
73 Kain BN, Luna P, Hormaechea Agulla D, Maneix L, Morales-Mantilla DE, Le D, et al. Specificity and heterogeneity of trained immunity in hematopoietic stem and progenitor cells. Blood. 2021;138(Supplement 1):2149–9.
74 Jeljeli M, Riccio LGC, Doridot L, Chene C, Nicco C, Chouzenoux S, et al. Trained immunity modulates inflammation-induced fibrosis. Nat Commun. 2019 Dec 11;10(1):5670.
75 Mills TS, Kain BN, Lucas ED, Burchill MT, Jiron Tamburini BA, King KY, et al. Hematopoietic stem cells undergo immune training and constitute a long-term reservoir for hyper-inflammatory macrophages in a mouse model of chronic autoimmunity. Blood. 2021;138(Supplement 1):2165–5.
76 Willis GR, Reis M, Gheinani AH, Fernandez-Gonzalez A, Taglauer ES, Yeung V, et al. Extracellular vesicles protect the neonatal lung from hyperoxic injury through the epigenetic and transcriptomic reprogramming of myeloid cells. Am J Respir Crit Care Med. 2021 Dec 15;204(12):1418–32.
77 Falcao-Holanda RB, Brunialti MKC, Jasiulionis MG, Salomao R. Epigenetic regulation in sepsis, role in pathophysiology and therapeutic perspective. Front Med. 2021;8:685333.
78 Riksen NP, Netea MG. Immunometabolic control of trained immunity. Mol Aspects Med. 2021 Feb;77:100897.
79 Bekkering S, Arts RJW, Novakovic B, Kourtzelis I, van der Heijden C, Li Y, et al. Metabolic induction of trained immunity through the mevalonate pathway. Cell. 2018 Jan 11;172(1–2):135–46.e9.
80 Emukah C, Dittmar E, Naqvi R, Martinez J, Corral A, Moreira A, et al. Mesenchymal stromal cell conditioned media for lung disease: a systematic review and meta-analysis of preclinical studies. Respir Res. 2019;20(1):239.
81 Liu FD, Tam K, Pishesha N, Poon Z, Van Vliet KJ. Improving hematopoietic recovery through modeling and modulation of the mesenchymal stromal cell secretome. Stem Cell Res Ther. 2018;9(1):268.
82 Wen S, Dooner M, Cheng Y, Papa E, Del Tatto M, Pereira M, et al. Mesenchymal stromal cell-derived extracellular vesicles rescue radiation damage to murine marrow hematopoietic cells. Leukemia. 2016 Nov;30(11):2221–31.
83 Infante A, Rodríguez CI. Secretome analysis of in vitro aged human mesenchymal stem cells reveals IGFBP7 as a putative factor for promoting osteogenesis. Sci Rep. 2018;8(1):4632.
84 Kohl V, Drews O, Costina V, Bierbaum M, Jawhar A, Roehl H, et al. Proteins marking the sequence of genotoxic signaling from irradiated mesenchymal stromal cells to CD34+ cells. Int J Mol Sci. 2021 May 29;22(11):5844.
85 How J, Hobbs GS, Mullally A. Mutant calreticulin in myeloproliferative neoplasms. Blood. 2019 Dec 19;134(25):2242–8.
86 Duo CC, Gong FY, He XY, Li YM, Wang J, Zhang JP, et al. Soluble calreticulin induces tumor necrosis factor-α (TNF-α) and interleukin (IL)-6 production by macrophages through mitogen-activated protein kinase (MAPK) and NFκB signaling pathways. Int J Mol Sci. 2014 Feb 20;15(2):2916–28.
87 Feng M, Marjon KD, Zhu F, Weissman-Tsukamoto R, Levett A, Sullivan K, et al. Programmed cell removal by calreticulin in tissue homeostasis and cancer. Nat Commun. 2018 Aug 10;9(1):3194.
88 Salati S, Prudente Z, Genovese E, Pennucci V, Rontauroli S, Bartalucci N, et al. Calreticulin affects hematopoietic stem/progenitor cell fate by impacting erythroid and megakaryocytic differentiation. Stem Cells Dev. 2018 Feb 15;27(4):225–36.
89 Netea MG, Joosten LA, Latz E, Mills KH, Natoli G, Stunnenberg HG, et al. Trained immunity: a program of innate immune memory in health and disease. Science. 2016 Apr 22;352(6284):aaf1098.